UCRL-ID-126011

Electrical Resistivity Monitoring of the Thermomechanical Heater Test in Yucca Mountain

A. Ramirez
W. Daily

February 19, 1998

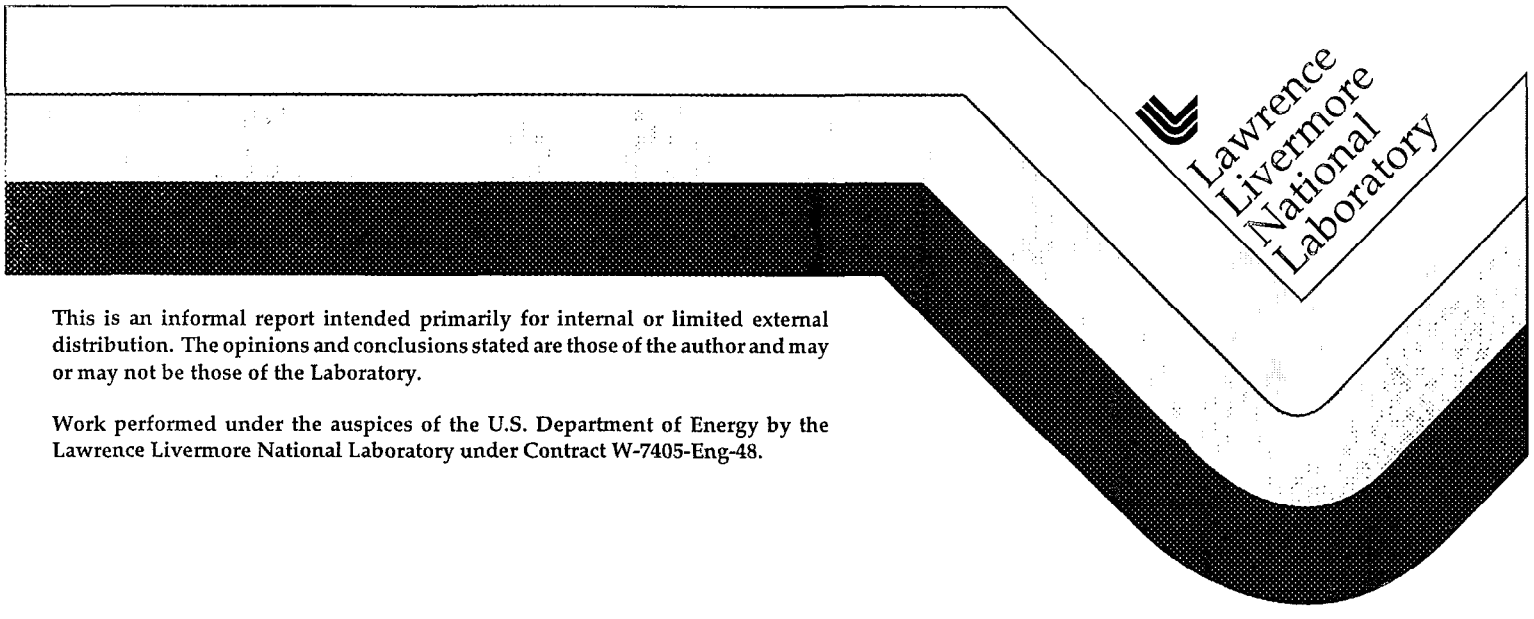

Work performed under the auspices of the U.S. Department of Energy by the Lawrence Livermore National Laboratory under Contract W-7405-Eng-48.

Electrical Resistivity Monitoring of the Thermomechanical Heater Test in Yucca Mountain

A. Ramirez, W. Daily
Lawrence Livermore National Laboratory

Abstract Of the several thermal, mechanical and hydrological measurements being used to monitor the rockmass response, electrical resistance tomography (ERT) is being used to monitor the movement of liquid water with a special interest in the movement of condensate out of the system. Four boreholes, containing a total of 30 ERT electrodes, were drilled to form the sides of a 30 foot square with the heater at the center and perpendicular to the plane of the electrodes. Images of resistivity change were calculated using data collected before and during the heating episode. The changes recovered show a region of decreasing resistivity approximately centered around the heater. The size this region grows with time and the resistivity decreases become stronger. The changes in resistivity are caused by both temperature and saturation changes. The Waxman Smits model has been used to calculate rock saturations after accounting for temperature effects. The saturation estimates suggest that a region of drying develops around the heater and grows over time. The estimates also show regions increase in saturation over time, primarily below and to the sides of the heater. The accuracy of the saturation estimates depends on several factors that are only partly understood at the time of writing.

Introduction

The single heater test (SHT) is one of the in situ thermal tests being conducted in the exploratory studies facility (ESF) in Yucca Mountain to enhance the understanding of the coupled processes. The primary objective of the SHT is to investigate the thermal-mechanical responses of the Topopah Spring tuff in Yucca Mountain.

This paper describes electrical resistance tomography (ERT) surveys made during the SHT in order to map the changes in moisture content caused by temperature changes. Of particular interest, is the formation and movement of condensate within the fractured rock mass.

The SHT is located off the Observation Drift about 40 m from the Main Tunnel of the ESF and about 2.8 km from the portal of the Tunnel. As shown in Figure 1, the heated block of the SHT is bounded by the Observation Drift and Thermal-mechanical Alcove Extension. One single element electrical heater was placed in a heater hole which was drilled horizontally into the heated block, at about the middle of the Thermal-mechanical Alcove at about 1.5 m from the floor. The total power output of the heater is about 4 kW. The heater element is about 5 m in length. The heated part of the heater hole starts at about 2 m from its collar. Four inclined boreholes were used to position electrodes around the region of interest forming a plane perpendicular to the heater axis at its center. Twenty

eight electrodes distributed among the 4 holes were used to conduct ERT surveys around the heater.

Electrical Resistance Tomography

Electrical resistance tomography (ERT) is a geophysical imaging technique which can be used to map subsurface resistivity. Rock mass heating creates temperature and liquid saturation changes which result in electrical resistivity changes that are readily measured. The ERT measurements consist of a series of voltage and current measurements from buried electrodes using an automated data collection system. The data are then processed to produce electrical resistivity tomographs using state of the art data inversion algorithms. We use these measurements to calculate tomographs that show the spatial distribution of the subsurface resistivities.

Here we describe briefly some of the important features of the two dimensional (2D) algorithm. For additional details, the reader is referred to Morelli and LaBrecque (1996). The algorithm solves both the forward and inverse problems. The forward problem is solved using a finite element technique in 2D. The inverse problem implements a regularized solution which minimizes an objective function. The objective of the inverse routine is to minimize the misfit between the forward modeling data and the field data, and a stabilizing functional of the parameters. The stabilizing functional is the solution's roughness. This means that the inverse procedure tries to find the smoothest resistivity model which fits the field data to a prescribed tolerance. Resistivity values assigned in this way to the finite element mesh constitute the ERT image. Although the mesh is of a large region around the electrode arrays, only the region inside the ERT electrode array is shown in the results because the region outside the array is poorly constrained by the data.

To calculate the changes in the rock's electrical resistivity we compared a data set obtained after heating started, and a corresponding data set obtained prior to heating. One may consider subtracting, pixel by pixel images from two different conditions. However, this approach could not be used because the resistivity structure was three-dimensional, i.e., several boreholes containing metallic instruments, were located near the plane of interest (see Figure 1). These metallic instruments caused large conductive anomalies and made the resistivity structure three dimensional (3D). The finite element forward solver cannot generate a model that will fit the data so the code chooses a solution with a poor fit. Our experience is that these effects can be reduced by inverting the quantity:

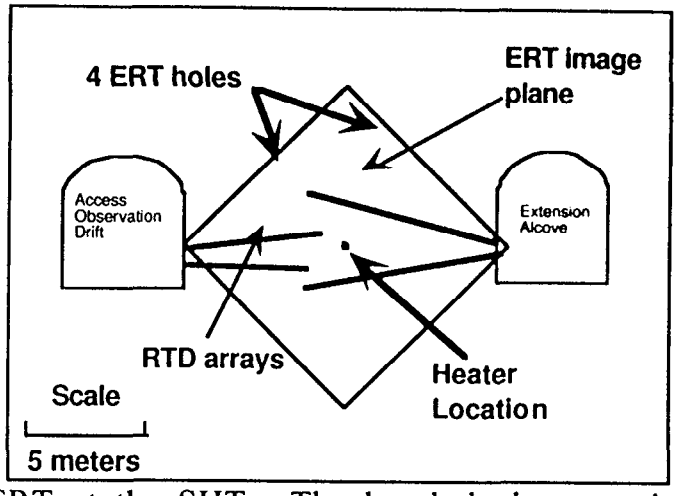

Figure 1. ERT at the SHT. The borehole layout relative to the drifts and the RTD boreholes is shown.

$$\frac{R_a}{R_b} \times R_h \qquad (1)$$

where R_a is the measured transfer resistance after heating started, R_b is the transfer resistance before heating and R_h is the calculated transfer resistance for a model of uniform resistivity. This approach tends to reduce the effects of anomalies which do not match the 2D assumptions of the resistivity model because the 3D effects cancel in the ratio since they are contained in both terms R_a and R_b.

The tomographs presented in this report were calculated in a somewhat different manner than the tomographs submitted previously. The data used for the tomographs in this report was the average of three consecutive data sets. That is, each reading used for the tomographs was the average value of the reading measured in three consecutive field surveys. We did this in order to improve the signal to noise ratio of the measurements made at low voltages.

Changes in Resistivity

An image for August 22 (not shown) changes detected using two data sets collected two hours apart. No changes were expected at this time because the heater was off (heating started on 8/26/96). Therefore, any changes observed in this image would be indicative of the effects of measurement error on the inversion process so that this image can be used to determine the significance of resistivity changes shown in subsequent images. On average, these "noise" images showed the resistivity ratio to deviate from 1.0 (i.e., perfect result when no changes occur) by +/-0.05. This analysis showed that changes of about 5% could be expected on the basis of measurement error. Therefore, the changes observed during heating need to be substantially bigger than 5% in order to be considered reliable.

The images from 8/29 and 9/3 in Figure 2 show changes 3 and 8 days respectively after heating started on 8/26. After just 3 days there is a weak conductive anomaly forming just below the heater but it is about 5% and therefore not statistically significant. On the other hand, on 9/3 changes are significant (up to 20% change) with a circular region of enhanced conductivity forming, not centered on the heater, but shifted about 1 m upward.

The rest of the images in Figure 2 show a clear trend of overall increase in electrical conductivity in the rockmass (decreasing resistivity or a ratio less than 1.0). However, the first 59 days of heating show a pattern of change which is different from the pattern observed in subsequent images. Prior to the December data the conductive anomaly is mostly circular in section (although not centered on the heater). However, after a 41 day data gap between October and December, the pattern is much more irregular and "fingers" begin to appear; the largest changes are near the heater but there is no clear pattern from which you could locate the heater. We believe that this is due to the fact that both saturation and temperature changes are influencing the resistivity ratios.

We interpret the later response (after day 59) as changes in moisture content due to drying and wetting along fracture systems. As the temperature increases above ambient, the vapor pressure in the pores increases and the vapor. Fractures connected pneumatically to the drift will provide a pressure gradient so that moisture will leave the rock along fracture surfaces and move along the fractures in response to buoyancy or thermally driven pressure gradients. The result will be dryer zones along fractures near the heater but wetter zones along fractures further away where temperature and pressure allow condensation below the local dew point. Interpretation of moisture content during this process is complicated by several factors. First, both moisture content and temperature affect the resistivity mapped by ERT. However, since we have a measure of temperature it is possible in principle to separate the two effects and we will attempt this in the next section. Second, our ERT inversion assumes the resistivity structure is strictly 2D such that the resistivity varies in the image plane but is constant perpendicular to the image plane (constant parallel to the heater axis). Therefore, the 2D assumption in our ERT model would probably mean a poor correlation between ERT image anomalies and fracture location (even if we had fracture maps for the rockmass volume). Despite these difficulties, it is safe to infer from the ERT images that after day 59 the fractures must play a significant role in rockmass moisture redistribution.

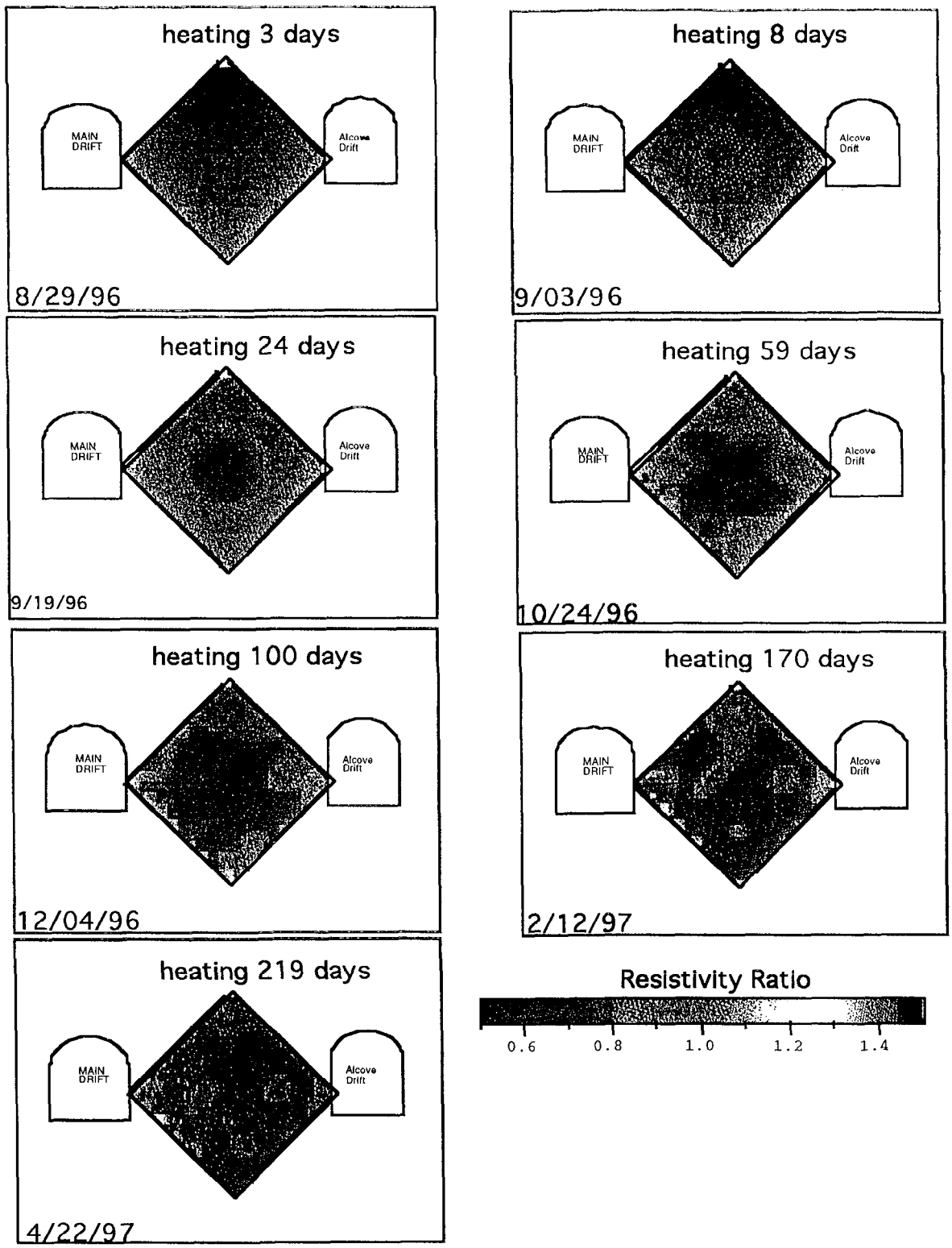

Figure 2. ERT sequence of resistivity changes from 8/29/96 to 4/2/97

Inferences of Moisture Changes from ERT

The resistivity changes in Figure 2 are influenced by changes in both moisture content and temperature: an increase in temperature or moisture causes a resistivity decrease. However, near the heater there may be regions where the increasing temperature which reduces the resistivity, acts opposite to the rock drying which increases the resistivity. Our goal in this section is to use the images of resistivity change near the heater, along with the measured temperature field and what is known of initial conditions in the rockmass to estimate moisture change during heating.

In order to estimate moisture content changes, we need to account for both effects of temperature, measured at many points by RTD's, and resistivity changes, measured by ERT. This is possible by either using laboratory data establishing the relations between moisture, temperature and resistivity or by using a suitable model of electrical conduction in porous media. Roberts and Lin (1997) have published data on the resistivity of Topopah Spring tuff as a function of moisture content. There is, however, limited data on temperature dependence (up to 95 C) and the samples were not from the SHT alcove so that direct use of this data is not simple to do. At a later date we will attempt to calibrate the Waxman Smits model with the laboratory data.

On the other hand, Waxman and Thomas (1954 a, 1954 b) describe a model for electrical conduction in partially saturated shales (intended for oil field data) which accounts for conduction through the bulk pore water as well as conduction through the electrical double layer near the pore surface. This model can predict temperature dependence of the resistivity but several of the model parameters are empirically determined and not available for tuff. Roberts and Lin suggest that the Waxman Smits model provides reasonably good estimates of resistivity for saturations greater than 20%. For saturations less than 20%, their data shows that the Waxman Smits model substantially underpredicts the resistivity. We will use this model to account for the temperature effects on the resistivity changes and to estimate changes in rock saturation.

Waxman begins with a parallel circuit model for conductance

$$C = \frac{1}{F^*}(C_w + BQ_v) \qquad (2)$$

where C is the conductivity or 1/R where R is the resistivity

F^* is the formation factor or ϕ^{-m} where ϕ is the porosity and m the porosity exponent

C_W is the pore water conductivity

B is the equivalent conductance of counterions on the double layer

Q_V is the effective concentration of exchange cations

The first term represents conductance through the bulk pore water while the second term is the conductance along the double layer. This expression can be modified for partially saturated media by realizing that the first term is just

Archie's equation and $Q/S = Q_V$ where S is the fractional saturation. In terms of resistivity we have equation (3) as

$$R = \frac{R_w \phi^{-m} S^{1-n}}{S + R_w B Q} \qquad (3)$$

where n is approximately 2, the saturation index in Archie's modified equation, and R_W is the water resistivity. Waxman and Thomas reported results that suggest that m is approximately equal to n. When $R_W BQ >> S$ the electrical double layer is the primary conduction pathway. When $R_W BQ << S$, the primary conduction pathway is through the open pore space.

We can use equation 3 in ratio form in order to calculate resistivity changes in the form of resistivity ratios. When the primary conduction pathway is the through the water in the open pore space, the resistivity ratio can be calculated as:

$$\frac{R_a}{R_b} = \frac{R_{w,a}}{R_{w,b}} \left(\frac{S_b}{S_a} \right)^2 \qquad (4)$$

where R_b and R_a are the resistivities before and after heating started, $R_{w,b}$ and $R_{w,a}$ are the water resistivities before and after heating. S_b and S_a are the saturations before and after heating started; we will refer to this case as model 1. This equation implies that the temperature dependence of the resistivity change is proportional to the change in water resistivity caused by temperature increases.

When the primary conduction pathway is through the electrical double layer, the ratio form of equation 3 simplifies to:

$$\frac{R_a}{R_b} = \frac{S_b}{S_a} \frac{B_b}{B_a} \qquad (5)$$

where B_b and B_a are the equivalent conductances of counter-ions in the electrical double layer; we will refer to this case as model 2. This equation implies that the temperature dependence of the resistivity ratio is caused by changes in counter-ion conductance due to temperature changes. Comparing equations 4 and 5, we see that the resistivity changes caused by saturation changes are largest for model 1 where the primary conduction pathway is through the pore space. We note that neither of these two models accounts for changes in water resistivity cause by rock/water chemical interactions. If chemical reactions cause large changes in the concentration or types of ions in the water, the estimated saturation changes will be in error.

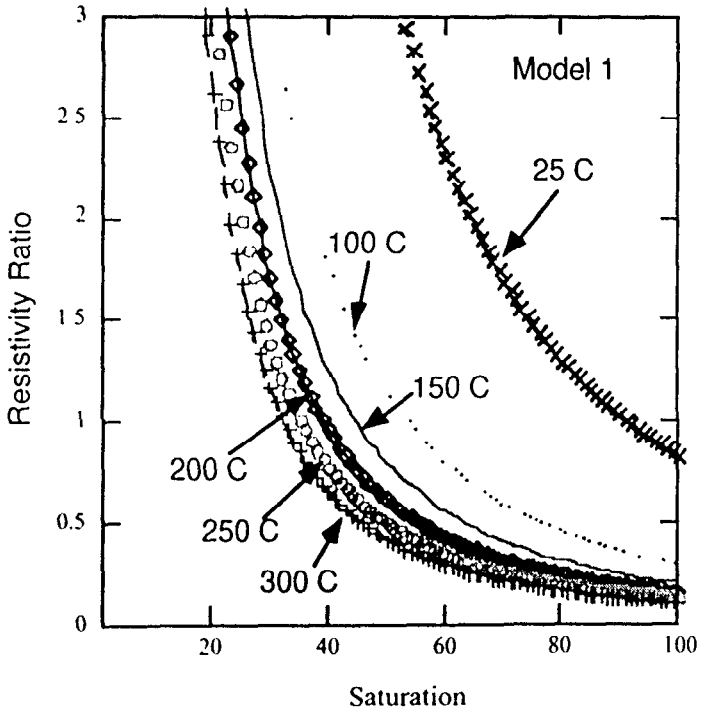

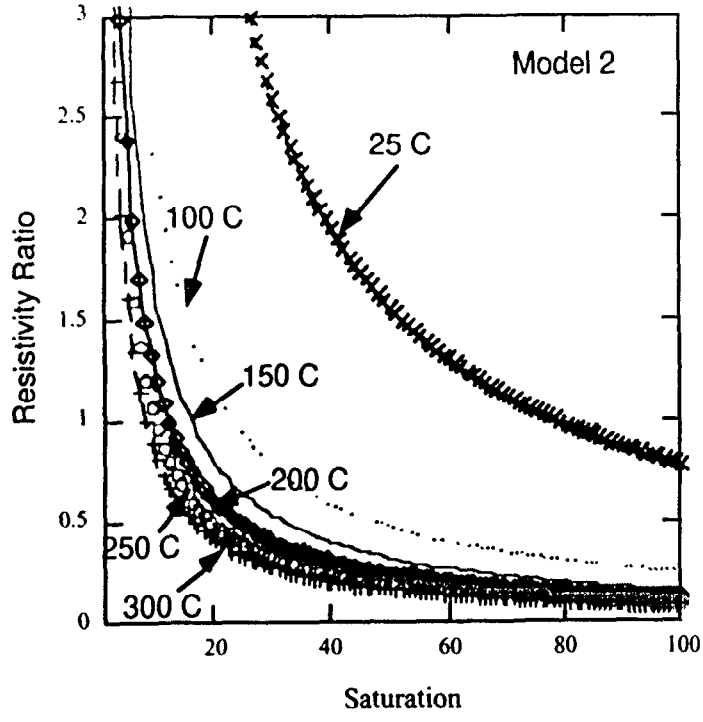

Figure 3 shows resistivity ratios as a function saturation for models 1 and 2. Curves representing the temperature range of 25 to 300 C are shown to illustrate the temperature and saturation dependence of the resistivity ratios.

We used the available temperature data to construct temperature maps along the ERT planes. It is necessary to have a reliable temperature measurement for each area (each tomograph pixel) were we wish to calculate the saturation change. At the SHT, there are many temperatures sensors located along roughly horizontal boreholes. However, the temperature coverage in the vertical direction is sparse extending only +/- 1.7 m away from the heater. In order to construct temperature maps we were forced to extrapolate vertically out to +/- 6.3 m away from the heater. It was necessary to assume that the vertical temperature gradient equaled the horizontal gradient in order to obtain physically reasonable temperature values for regions beyond 1.7 m vertically. Thus, the accuracy of the temperature maps is expected to be good along the horizontal direction but may be in error along the vertical direction for regions farther than 1.7 meters from the heater.

The ERT images provide a measure of change in R from baseline (through the resistivity ratio). Equations 4 and 5 can be used to relate electrical resistivity changes to changes in saturation when the temperatures are known and the temperature dependence of R_W and B can be calculated. Since the magnitude of R_WBQ is changing in space and time we have chosen to estimate the changes in saturation by using both model 1 and 2. This approach should provide bounds to the domain of possible saturations that may be present. Available data suggests that the welded at the SHT should show behavior closer to model 2 than to model 1. Assuming average values of cation exchange capacity for welded tuff of about 3 meq/100 g, porosity of 0.10 (porosity is used to calculate Q) and R_W =39 ohm-m at 25 C (resistivity of J-13 water), it can be shown that R_WBQ is about 23 at 25 C and that it increases with temperature. Given that S ranges from 0.0 to 1.0, this result suggests that R_WBQ is >> S and thus that the primary pathway for conduction at the SHT is the electrical double layer. Therefore, we believe that the results of model 2 are probably closer to reality. However, if the cation exchange capacity, porosity or water resistivity varied significantly across the ERT image plane, it is possible that model 1 results may be closer to reality. The results of these saturation estimates are discussed next.

Figure 4 shows estimates of saturation based on the resistivity ratios and interpolated/extrapolated maps of temperature. The color scale for the resistivity ratios has been changed from that used in Figure 2 in order to emphasize the regions which show the highest reduction in resistivity. The temperature maps were used to calculate the temperature dependent properties on models 1 and 2 (R_W, B) We will assume that initial saturation (S_b) of the rock unit was 0.92; this is the average saturation from core samples collected at the experimental site and reported by Wagner (1996). Both models indicate that the saturation around the heater decreased as heating time increased. Model 2 generally predicts substantially drier saturations near the heater than model 1; model 2 saturations near the heater are closer to a priori expectations than those from model 1. As time increased, the drying zone appears to propagate upwards especially after 219 days of heating; also the minimum saturation estimate is near 0.1 (model 2).

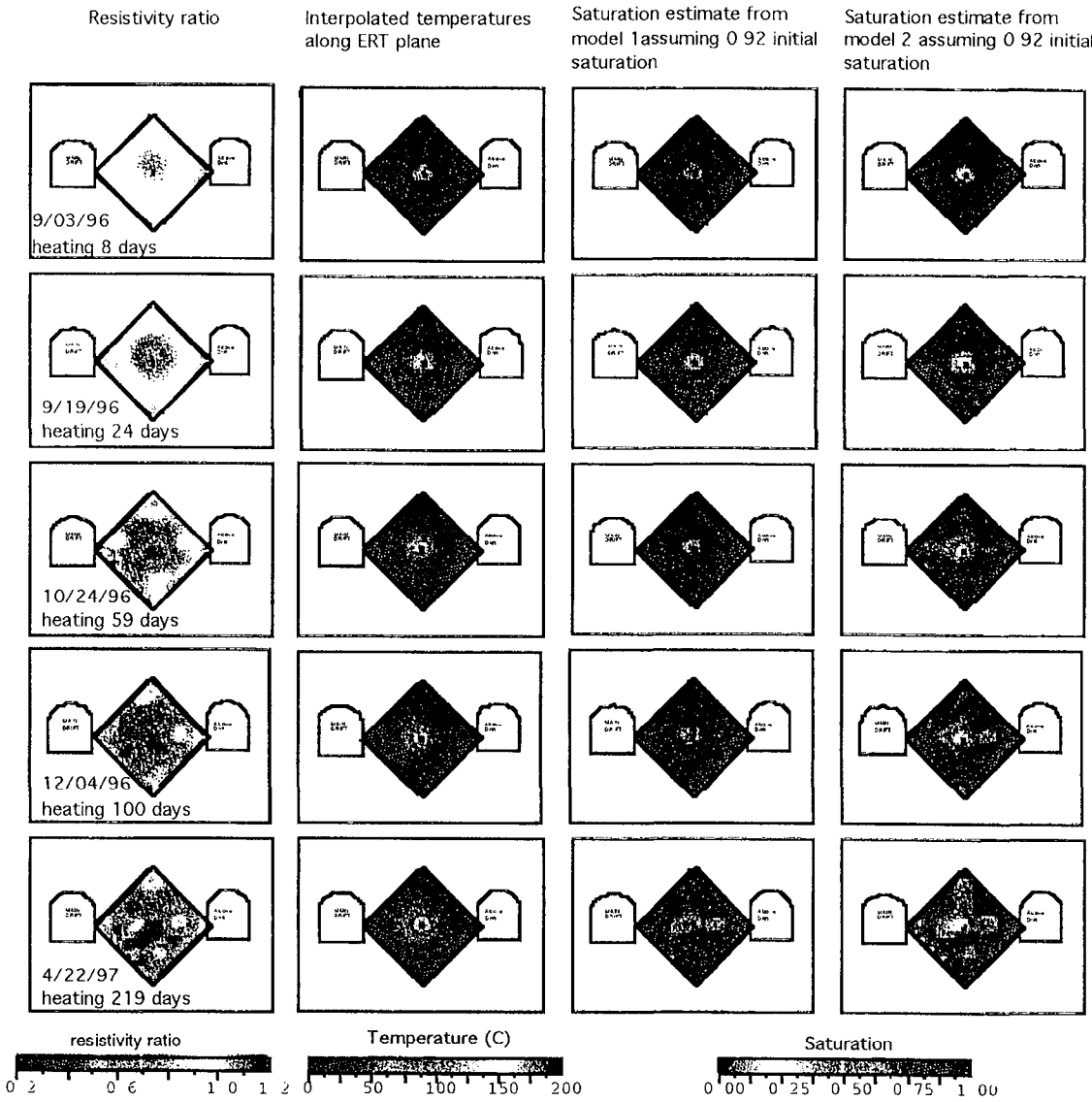

Figure 4 Shows the resistivity ratio tomographs, corresponding temperature maps and estimates of saturations corresponding to models 1 and 2. Note that the color scale used for the resistivity ratios is different than that used for Figure 2 in order to emphasize the lowest resistivity ratios measured.

Figure 5 presents our interpretation of where the rock is losing or gaining moisture as a function of time. The drying and wetting regions in Figure 5 are based on tracings made over the tomographs in Figure 4. Figure 5 helps illustrate the moisture behavior implied by the model 2 results and amplifies the scale for clearer viewing. The wetting behavior of the rock appears to change over time. Model 2 results for 9/03/96 show saturations near 1.0 for a small pocket of rock about 1 m directly above the heater. This pocket of increased saturation disappears by 9/19/96. Pockets of the rock below the heater appears to reach full saturation (purple color) around day 59, near the 7 o'clock and 8 o'clock positions. Around day 100, portions of the rock near the 2 o'clock and 4 o'clock position reach full saturation in model 2. After 219 days most of the rock

below the heater appears to be at or near full saturation, whereas above the heater there are only a few pockets at full saturation. The shape defined by the full saturation zone after 219 days is roughly that of a "U". This shape would suggest that the primary zone of condensate accumulation is down and to either side of the heater. The model 2 saturation estimates suggest that the rock above the heater is becoming drier while the rock below the heater is becoming wetter. The drying zone appears to form pockets as it grows. We speculate that these pockets may be caused by heterogeneities in the rock such as fractures. Similar comments can be made regarding the wetting zones shown. A wetting zone located near the left drift (Access Observation Drift) is not well understood; this wetting zone may be unrelated to the effects of heating and may possibly be caused by other underground activities.

The saturation estimates presented are considered to be "rough" estimates. At the time of writing, we continue to work to understand and improve the saturation estimates in Figure 4. The accuracy of the saturation estimates in Figure 4 may be limited by one or more of the following factors. 1) The accuracy of the temperature maps in the vertical direction is limited by the sparse vertical coverage of the temperature sensors. Errors in the interpolated/extrapolated temperature maps will result in erroneous saturation estimates. 2) The effects of rock/water interactions on electrical resistivity are not accounted for by the Waxman Smits model. This means that if significant changes develop in the number or types of ions in solution may cause resistivity changes that the model would treat as saturation changes. Data from SHT water samples may be helpful in understanding this effect. 3) Laboratory measurements of the electrical resistivity of welded tuff (Roberts and Lin, 1997) indicate that the Waxman Smits model underpredicts resistivity for saturations below 20 %. The saturation estimates below 20 % in Figure 4 are affected by this limitation. Attempts are currently underway to "calibrate" the Waxman Smits model with the laboratory data. 4) Work by Llera et al. suggest that growth of microcracks at high temperature can affect electrical resistivity of welded tuff; this effect, if present at the SHT, is not accounted for by the Waxman Smits model. 4) The resistivity ratios were calculated using a 2D algorithm whereas natural heterogeneities such as fractures are likely 3D. Changes in resistivity occurring along fractures may be distorted. 5) Several boreholes containing metallic instruments are located near the plane of interest. These metallic instruments caused large conductive anomalies may reduce sensitivity to resistivity changes occurring in the rock thereby resulting in resistivity change tomographs which show smaller change than those present in the rock.

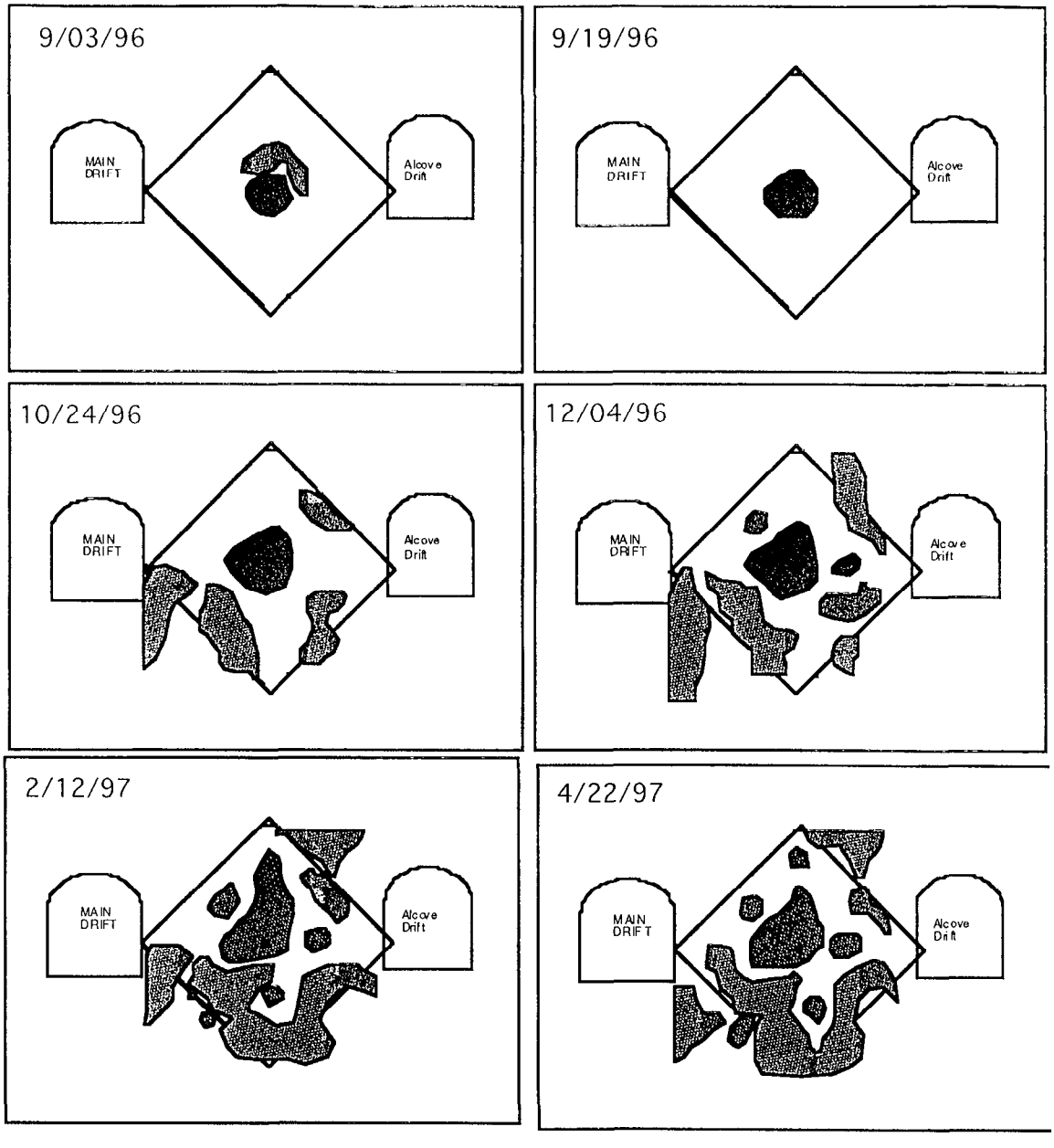

wetting regions drying regions

Figure 5 shows regions were drying and wetting is ocurring as interpreted from the model 2 moisture estimates

Summary and Conclusions:

To calculate the changes in the rock's electrical resistivity we compared a data set obtained after heating started, and a corresponding data set obtained prior to heating. We see a region of decreasing resistivity approximately centered around the heater. The size of this region grows with time and the resistivity decreases become stronger. At this point the changes in resistivity are caused mostly by increasing temperature of the rockmass pore water although and

saturation changes also play a role. The early tomographs show a radially symmetric anomaly centered just below the heater; the largest resistivity changes occur closest to the heater. This pattern persists for at least 59 days of heating. We suggest that the differences in behavior of the condensate above and below the heater are probably the cause of the asymmetry. To this point it is likely that our images are not dominated by drying along fractures. At later times the shape of the anomalies becomes more like fingers. We believe that heterogeneities in the rock such as fractures are affecting the drying and wetting fronts at these later times thereby affecting the shape of the anomaly.

Saturation estimates have been presented. These estimates were calculated from two models derived from the Waxman Smits equation. Of the two models considered, we believe that the model that assumes dominant surface conductance (model 2) provides the most accurate estimates. The saturation estimates show a region of drying developing around the heater and growing with heating time. The drying region appears to propagate upwards and sideways. Early on during heating, the saturation appears to increase above the heater. This increase later disappears while the rock below and to the sides of the heater shows saturation increases. The saturation estimates are considered "rough" estimates, and work is ongoing to better understand and improve these. Several factors which may be affecting the accuracy of the estimates have been identified.

Acknowledgments:
This work is performed under the auspices of the U.S. Department of Energy by Lawrence Livermore National Laboratory under contract W-7405-ENG-48. This work is supported by Yucca Mountain Site Characterization Project, LLNL.

References

Llera, F., M Sato, K. Nakasuka, and H. Yokohama, 1990, Temperature Dependence of the electrical resistivity of water saturated rocks., *Geophysics*, vol. 55, no 5., pp. 576-585.

Roberts, J. and W. Lin, 1997, Electrical properties of partially saturated Topopah Spring tuff: Water distribution as a function of saturation, *Water Resources Research, 33*,577-587.

Wagner, R. A., 1996, Characterization of the ESF Thermal Test Area, TRW Inc, Yucca Mountain Site Characterization Project, Las Vegas NV, B00000000-0717-5705-00047 Rev 01.

Waxman, M.H. and E.C. Thomas, 1974 a, "Electrical Conductivities in Shaly Sands - I. The Relation Between Hydrocarbon Saturation and Resistivity Index; The Relationship between Hydrocarbon Saturation and Resistivity Index," *Journal of Petroleum Technology* (Feb.) 213-218; Transactions AIME, 257.

Waxman, M.H. and E.C. Thomas, 1974 b, "Electrical Conductivities in Shaly Sands - II. The Relation Between Hydrocarbon Saturation and Resistivity Index;

II. The Temperature Coefficient of Electrical Conductivity," *Journal of Petroleum Technology* (Feb.) 218-225; Transactions AIME, 257.

Technical Information Department • **Lawrence Livermore National Laboratory**
University of California • Livermore, California 94551